Research Paper

Decreased autophagy and fuel switching occur in a senescent hepatic cell model system

Brijesh Kumar Singh[1], Madhulika Tripathi[1], Reddemma Sandireddy[1], Keziah Tikno[1], Jin Zhou[1], Paul Michael Yen[1,2]

[1]Cardiovascular and Metabolic Disorders Program, Duke-NUS Medical School, Singapore 169857, Singapore
[2]Duke University School of Medicine, Durham, NC 27710, USA

Correspondence to: Brijesh Kumar Singh; **email:** singhbrijeshk@duke-nus.edu.sg
Keywords: aging, liver, senescence, metabolism, AML12 cells
Received: April 23, 2020 **Accepted:** June 18, 2020 **Published:** July 26, 2020

ABSTRACT

Although aging in the liver contributes to the development of chronic liver diseases such as NAFLD and insulin resistance, little is known about the molecular and metabolic details of aging in hepatic cells. To examine these issues, we used sequential oxidative stress with hydrogen peroxide to induce premature senescence in AML12 hepatic cells. The senescent cells exhibited molecular and metabolic signatures, increased SA-βGal and γH2A.X staining, and elevated senescence and pro-inflammatory gene expression that resembled livers from aged mice. Metabolic phenotyping showed fuel switching towards glycolysis and mitochondrial glutamine oxidation as well as impaired energy production. The senescent AML12 cells also had increased mTOR signaling and decreased autophagy which likely contributed to the fuel switching from β-oxidation that occurred in normal AML12 cells. Additionally, senescence-associated secretory phenotype (SASP) proteins from conditioned media of senescent cells sensitized normal AML12 cells to palmitate-induced toxicity, a known pathological effect of hepatic aging. In summary, we have generated senescent AML12 cells which displayed the molecular hallmarks of aging and also exhibited the aberrant metabolic phenotype, mitochondrial function, and cell signaling that occur in the aged liver.

INTRODUCTION

Aging is a major risk factor for many chronic diseases. In the liver, aging increases the susceptibility towards acute liver injury and hepatic fibrotic response [1–3]. Moreover, aging has been positively associated with increased risk and poor prognosis of various liver diseases including non-alcoholic fatty liver disease (NAFLD), insulin resistance, alcoholic liver disease, hepatitis C, and negatively associated with hepatic regenerative capacity [3, 4]. Currently, the study of aging and chronic hepatic diseases has been hampered by the long period of time necessary to conduct human and animal studies and the limited relevance of non-mammalian models to human diseases. While there are *in vitro* aging models that employ fibroblasts, there currently are no reliable *in vitro* hepatic cell models to study aging in the liver.

Cellular senescence is the main feature manifested in tissues of the aging organism [1, 5–8]. It is characterized by permanent cell cycle arrest, resistance to apoptosis, and a senescence-associated secretory phenotype [5]. Under pathological stress conditions, excessive accumulation of senescent cells in affected tissues adversely affects their regenerative ability and creates a pro-inflammatory environment that can resemble those found in age-related disorders such as Alzheimer's disease, cardiovascular disease, type 2 diabetes, and other conditions including chronic liver diseases [3, 5, 7, 9–12]. Targeting senescent cells has the potential to delay age-associated disorders and/or

reverse pathological metabolic phenotypes [3, 13–16]. Recent studies in the liver show that inducing hepatocyte senescence promotes fat accumulation and hepatic steatosis *in vitro* and *in vivo* [17]. Likewise, targeting senescent hepatocytes and adipocytes reduces overall hepatic steatosis and improves obesity-induced metabolic dysfunction [14, 17]. These findings suggest that senescence plays an important role in the development of chronic hepatic diseases and their metabolic abnormalities.

Previous senescent cell models have used primary fibroblast or hepatic cancer cells that were subjected to oxidative stress [18–22], or primary hepatocytes that underwent gamma irradiation [17]. However, these models have certain limitations since different cell types will react differently to a given stressor [23]. Furthermore, the method of senescence induction *i.e.*, oxidative stress, gamma irradiation, or overexpression of an oncogene, may contribute to variable phenotypes that may not necessarily resemble aging *in vivo* [5, 16, 23]. Thus, it is critical to compare and verify the fidelity of *in vitro* models with tissues from aged mice. Although there remains some uncertainty about the optimal method to induce senescence *in vitro*; it generally is agreed that oxidative stress and mitochondrial dysfunction play significant roles in the aging process [6, 11, 24, 25]. Using repetitive H_2O_2 exposures, we generated hepatic cellular senescence in hepatic Alpha Mouse Liver 12 (AML12) cells. Our characterization of the senescent cells showed that these senescent AML12 cells exhibited age-related molecular and metabolic changes, particularly a fuel switch to glycolysis and glutamate oxidation and decreased autophagy found in the livers of aged mice.

RESULTS

Senescence induction and validation in AML12 cells

AML12 cells were grown to 50% confluency and then treated with 1 mM H_2O_2 for 1 h for one day. They subsequently were treated with 750 μM H_2O_2 in serum-free DMEM:F12 medium for 1 h per day for 5 consecutive days as described in Figure 1A. After each treatment, serum-free DMEM:F12 medium containing H_2O_2 was replaced with complete DMEM:F12 medium (containing 10% FBS, 1x ITS, 100 nM dexamethasone, and 1x penicillin and streptomycin) for a 23 h period of recovery during each day. Cells then were sub-cultured/re-seeded in the ratio of 1:3 until they reached confluency >80% after approximately 3 days. As shown in Figure 1B, morphological effects such as cellular hypertrophy were observed after 2 days of H_2O_2 treatment. After 6 days of multiple H_2O_2 treatments, the cells showed classical features of senescence as they were distinctly larger and showed less proliferation than untreated controls (Figure 1B, 1C) [8]. Moreover, the mRNA expression of senescence marker genes, *TP53/p53*, *CDKN2A/p21*, and *CDKN1A/p16* were increased in the senescent AML12 cells compared to control AML12 cells (Figure 1D). Similarly, the expression of these genes also was increased in livers from old mice (100-108 weeks age) compared to those from young mice (12-20 week age) (Figure 1E). Furthermore, multiple H_2O_2 treatments increased senescence since there was increased activated β-Gal (SA β-Gal)-positive cells (Figure 2A, 2B), Both γH2A.X-positive cells containing condensed chromatin in larger nuclei and cellular hypertrophy were increased in treated cells (Figure 2C–2F). Taken together, these data showed that multiple H_2O_2 treatments markedly induced premature senescence in AML12 cells [1]. Consistent with these findings, RNAseq analysis in these AML12 cells also showed that cellular senescence and aging pathways such as inhibition of apoptosis signaling and the positive regulation of senescence and aging, generation of superoxide anions, and inflammatory response were significantly upregulated in senescent AML12 cells (Supplementary Figure 1A).

Bioenergetic phenotype of senescent AML12 cells

To perform the bioenergetic phenotyping of senescent AML12 cells, we used the Seahorse extracellular flux analyzer to measure the cell's glycolytic and oxidative potential. Senescent AML12 cells showed a higher oxygen consumption rate (OCR) and extracellular acidification rate (ECAR) than control cells (Figure 3A). Senescent AML12 cells also were more reliant on glycolysis for cellular energy than oxidative metabolism under energy stress conditions (Figure 3B). We further analyzed the glycolytic potential of senescent AML12 cells and found that they had significantly higher basal glycolysis, glycolytic potential as well as glycolytic reserve capacity than control cells (Figure 3C, 3D). Furthermore, senescent AML12 cells had marked increases in basal mitochondrial activity and maximum respiratory capacity, but no change in mitochondrial ATP production (Figure 4A, 4B). Instead, these cells showed reduced coupling efficiency and increased proton leak, suggesting they had mitochondrial dysfunction, a hallmark of cellular senescence and aging. Finally, mitochondrial fuel oxidation analysis showed there were significant reductions in glucose and fatty acid flexibilities and capacities. In contrast, there was an enhancement of glutamine oxidation flexibility and capacity (Figure 4C). Interestingly, glutamine-associated oxidation pathways also were upregulated in RNAseq analysis in these cells (Supplementary Figure 1A, Supplementary Data-RNAseq Pathway analysis in Pathways Up). However, there were no significant changes

in glucose, fatty acid, or glutamine oxidation dependency (Figure 4C).

Molecular phenotyping of energy sensing molecules in senescent AML12 cells

We next analyzed the activation (via phosphorylation) of several key energy-sensing proteins: AMPK, AKT, mTOR, p70S6K (mTOR target), as well as the formation of LC3B-II and p62 (autophagy-related proteins) in senescent AML12 cells by Western blotting. As a signature of senescent cells, we observed marked increases in the phosphorylation of AMPK, AKT, mTOR, and p70S6K proteins in senescent AML12 cells (Figure 5A, 5B). This phosphorylation pattern was similar to the one observed in the livers of aged mice (Figure 5C, 5D). Furthermore, RNAseq pathway analysis also showed several insulin-related

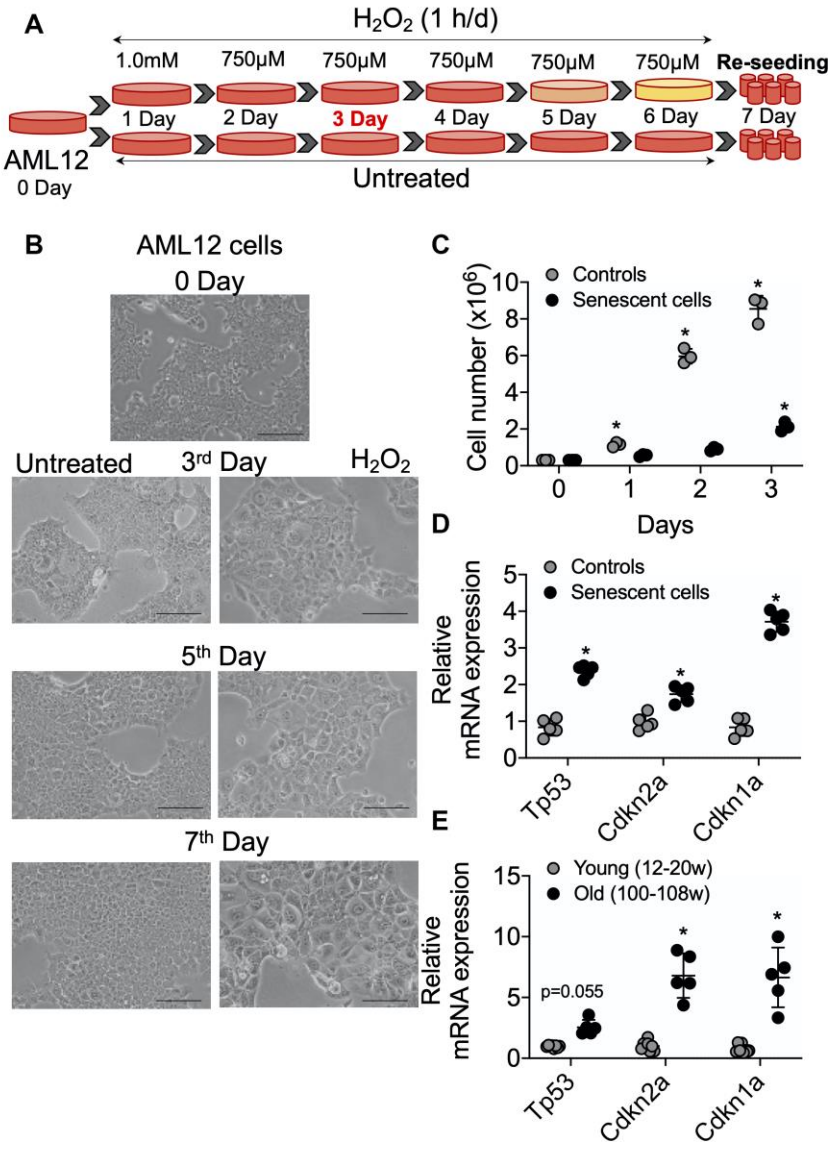

Figure 1. Senescence induction in mice normal hepatic cells AML12. (**A**) Schematic representation of experimental strategy for the senescence induction. 4x10^6 Cells were seeded at day 0 in the T175 cell culture flask. Next day (day 1) cells were treated with 1.0 mM H_2O_2 followed by 750 μM for the subsequent 5 days. Cells can be sub-cultured at 1:3 ratio on day 3 if required. At day 7, cells were re-seeded for experiments as required. (**B**) Visualization of senescence induction in mice AML12 cells during H_2O_2 treatments from day 3, day 5, and day 7 before re-seeding. The images are taken randomly at 10x magnification. Scale bars as 100 μm. (**C**) 0.3x10^6 control and senescent AML12 cells were seeded in each well of the 6-well plate. Cells were trypsinized at indicated days and counted by an automated cell counter. (**D** and **E**) RT-qPCR analysis of senescence genes in AML12 cells (**D**) and liver tissues from young and old mice (**E**). * Statistical differences were calculated significant as $p<0.05$.

pathways along with prolong ERK1/2 and MAPK signaling pathways were upregulated (Supplementary Figure 1B, 1C, Supplementary Data-RNAseq Pathway analysis> Pathways Up), while negative regulation of mTOR signaling was downregulated (Supplementary Figure 2C, Supplementary Data RNAseq Pathway analysis in Pathways Down). Additionally, we observed a marked increase in the expression of autophagy proteins, LC3B-II and P62, under basal conditions suggesting there was a late autophagic block in both the senescent AML12 cells and livers from aged mice. Furthermore, we showed that there was a decrease in autophagy flux in senescent AML12 cells by treating senescent and normal AML12 cells with a lysosome

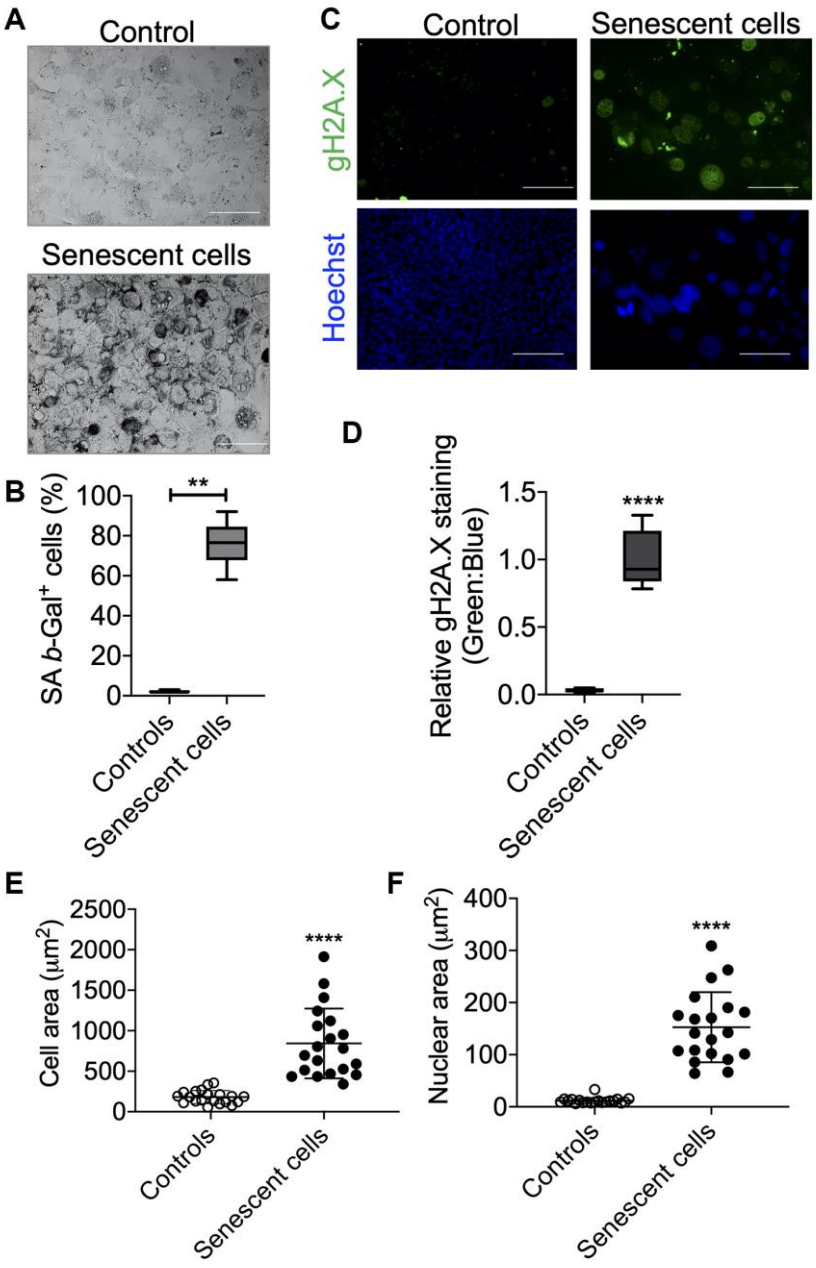

Figure 2. Senescence validation by SA β-Gal and γH2A.X staining. After senescence induction at day 7, cells were re-seeded in 4-chambered slides and next day SA β-Gal (**A**) and γH2A.X (**B**) staining were performed. Cells were counted manually for analyzing SA β-Gal+ cells over total cells and presented as percent positive cells. Scale bars as 50 μm. (**C**) Cells were counter-stained with Hoechst 33324 for immunofluorescence imaging and relative γH2A.X signals were analyzed over Hoechst 33324 signals. Scale bars as 100 μm. (**D**). (**E** and **F**). Area of the cells (**E**) and nucleus (**F**) were measured using ImageJ (NIH) software. Statistical differences were calculated significant as *p<0.05 and **p<0.001.

inhibitor, bafilomycin A1 (Figure 5E–5F). Densitometric analysis showed that LC3B-II accumulation was less in senescent than normal AML12 cells. We also observed an accumulation of neutral lipids in senescent AML12 cells at basal conditions that was similar to the increased hepatic triglyceride content found in aged mice (Figure 5G–5I). Of note, RNAseq pathway analysis also showed that several pathways regulating lipid handling, catabolism along with triglyceride catabolic pathways were downregulated (Supplementary Figure 2A, Supplementary Data-RNAseq Pathway analysis in Pathways Down).

Senescent AML12 cells create a pro-inflammatory environment and sensitize healthy AML12 cell towards pathological damage

Senescent cells secrete senescence-associated secretory proteins such as IL6 and IL1-β. These secreted proteins are thought to be responsible for creating a pro-inflammatory environment for neighboring cells during aging-associated diseases [1, 26, 27]. We found that senescent AML12 cells showed higher expression of the pro-inflammatory genes, *IL1b* and *IL6* (Figure 6A). Similarly, liver tissue from old mice showed

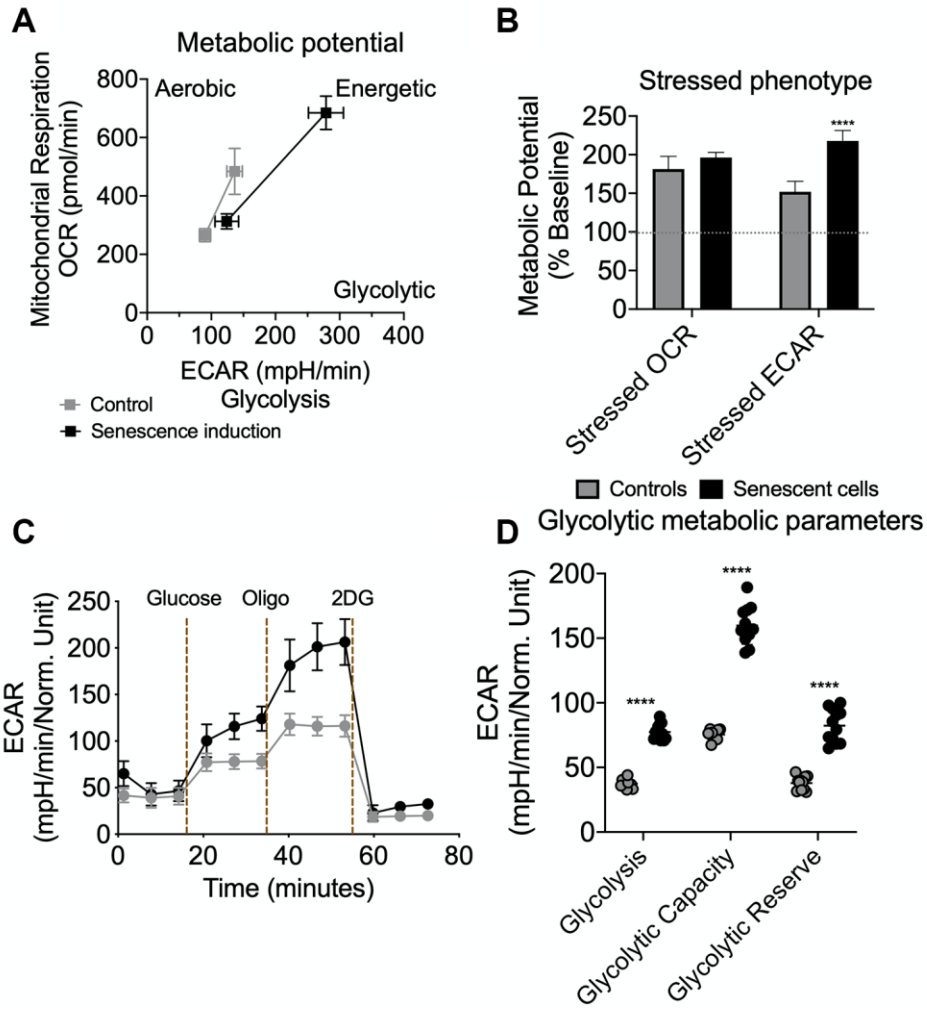

Figure 3. Seahorse extracellular flux analysis for metabolic potential and glycolytic flux in senescent AML12 cells. Agilent Seahorse XF Cell Energy Phenotype Test kit was used with Agilent Seahorse XFe96 Extracellular Flux Analyzer to analyze control and senescent AML12 cell's metabolic potential (**A**) and stressed phenotype (**B**). Oxygen consumption rate (OCR) represents mitochondrial respiration while the extracellular acidification rate (ECAR) represents glycolytic potential under basal and stressed conditions (as described in Methods) (**A**). Percent change in mitochondrial oxidative phenotype (OCR) and glycolytic phenotype (ECAR) under stress over basal (100%) conditions (**B**). Agilent Seahorse XF Glycolysis Stress Test kit was used with Agilent Seahorse XFe96 Extracellular Flux Analyzer to analyze control and senescent AML12 cell's glycolytic flux and reserve capacity (**C**). Glycolytic metabolic parameters were calculated as described in the Methods (**D**). All the parameters presented in the panel **B** and **D** were calculated using Seahorse Wave Desktop software. Statistical differences were calculated significant as **p<0.01; ****p<0.0001.

significantly higher expressions of *IL1b* and *IL6* mRNA (Figure 6B). We next treated control AML12 cells with conditioned media collected from senescent AML12 cell cultures, and found that they not only increased the expression of inflammatory (*IL1b*, *IL6*, *CCL2*) and fibrosis (*IL11*) genes in normal AML12 cells but also increased the latter's sensitivity to induction of inflammatory (*IL1b*, *IL6*, *CCL2*) and fibrosis (*IL11*) genes by saturated fatty acids (palmitate 0.5 mM for 24 h) in comparison to conditioned media prepared from control AML12 cell cultures (Figure 6C). Interestingly, RNAseq pathway analysis revealed that IL1b production and IL1b secretory pathways as well as with extracellular matrix-related pathways were significantly upregulated (Supplementary Figure 1D, Supplementary data-RNAseq Pathway analysis> Pathways Up). Furthermore, superoxide generation unfolded protein response (UPR), TNF-mediated signaling, chemokine secretion pathways, and the urea cycle were significantly upregulated (Supplementary Figure 1A, Supplementary Data-RNAseq Pathway analysis in Pathways Up). While, several glutathione metabolism regulating REDOX pathways along with nuclear receptors transcription pathways were significantly downregulated (Supplementary Figure 2B, 2C, Supplementary Data-RNAseq Pathway analysis in Pathways Down).

DISCUSSION

Cellular senescence significantly increases in most tissues during aging [9, 12, 24]. Previous *in vitro* senescence models have utilized primary fibroblasts or hepatic carcinoma cells that were subjected to oxidative stress conditions or irradiation [17–23]. However, these models have limited application to the aging liver due to differences in their respective molecular and metabolic phenotypes. Since oxidative stress and mitochondrial dysfunction are considered to be critical for senescence and aging [6, 11, 24, 25], we subjected non-transformed AML12 hepatic cells to multiple exposures of sublethal H_2O_2 to induce premature cellular senescence to study

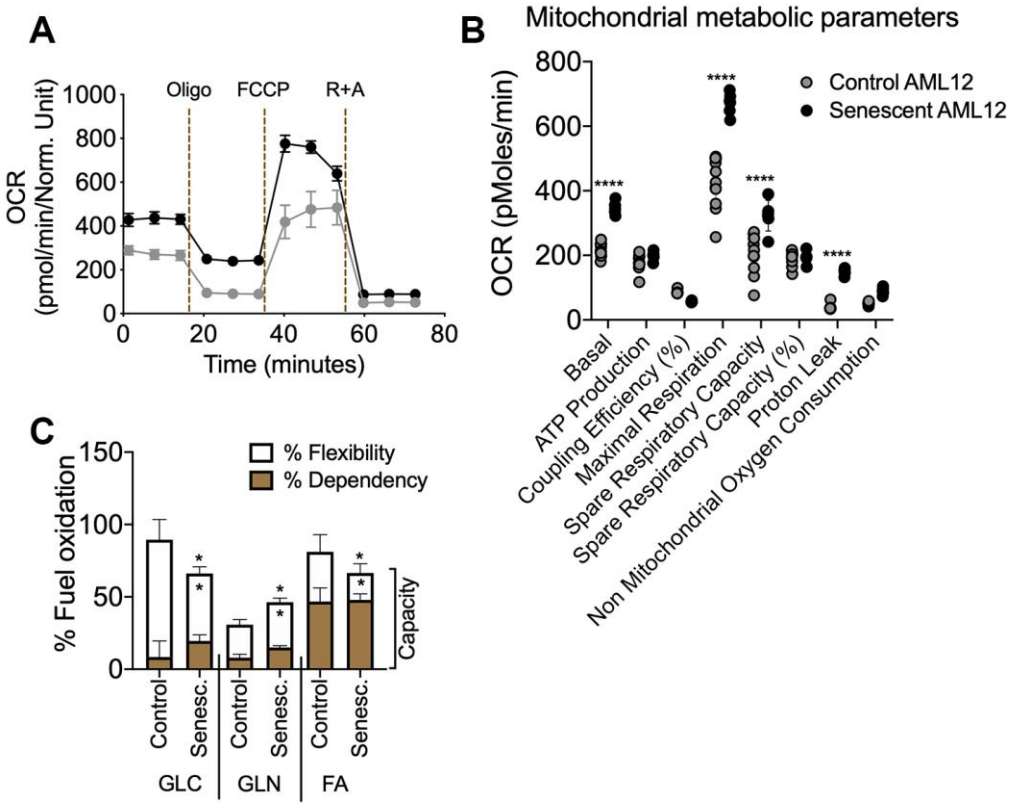

Figure 4. Seahorse extracellular flux analysis for mitochondrial metabolic parameters and fuel oxidation in senescent AML12 cells. Agilent Seahorse XF Mito Stress Test kit was used with Agilent Seahorse XFe96 Extracellular Flux Analyzer to analyze control and senescent AML12 cell's mitochondrial metabolic potential (**A** and **B**). (**C**) Agilent Seahorse XF Mito Fuel Flex kit was used with Agilent Seahorse XFe96 Extracellular Flux Analyzer to analyze control and senescent AML12 cell's mitochondrial fuel (glucose, glutamine, and fatty acids) oxidation. All the parameters presented in the panel **B** and **C** were calculated using Seahorse Wave Desktop software. Statistical differences were calculated significant as *p<0.05 and ****p<0.0001.

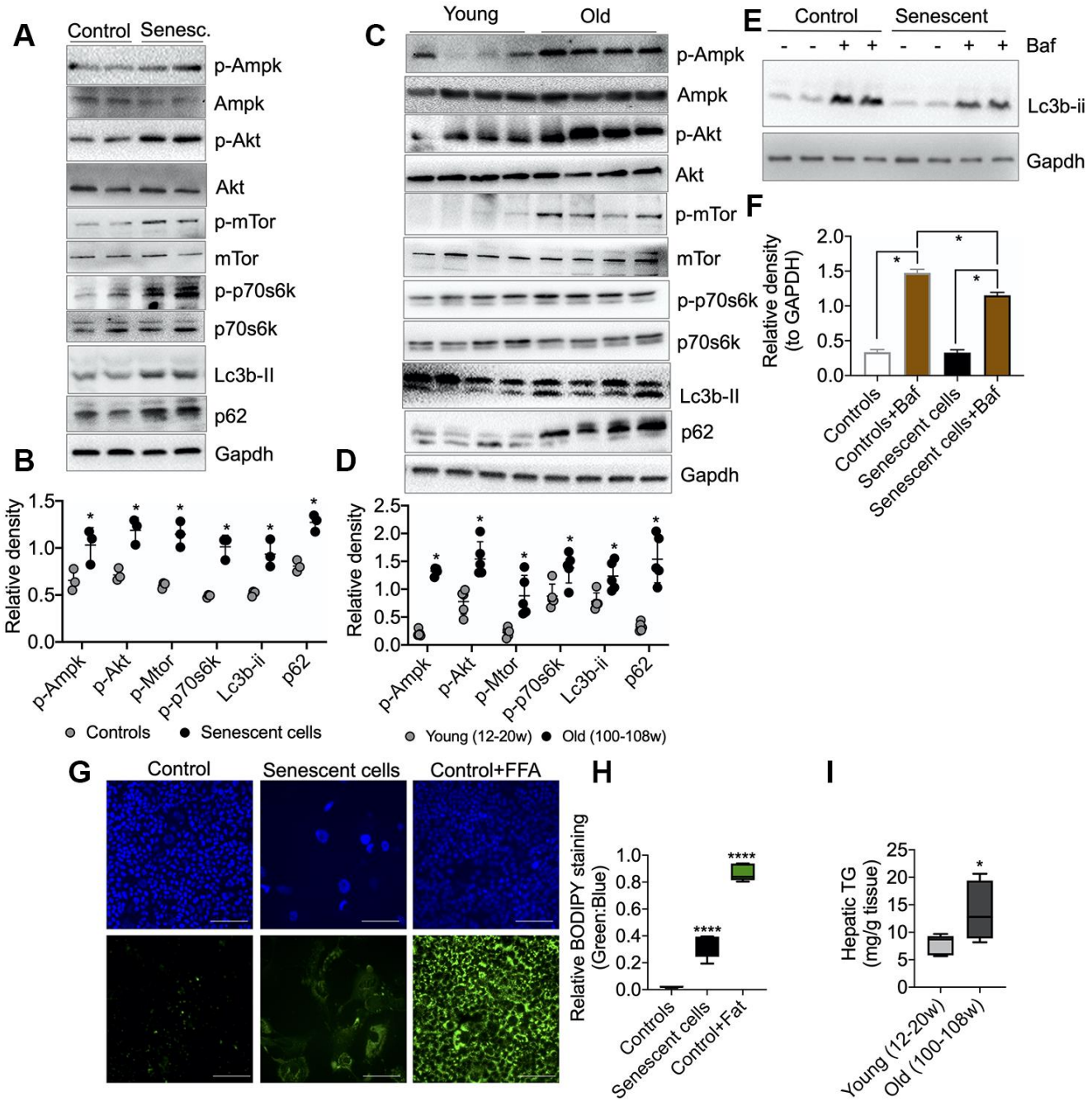

Figure 5. Molecular analysis of energy-sensing pathways in senescent AML12 cells and liver tissues from young and old mice. (**A**) Western blot analysis of energy sensing and autophagic proteins including GAPDH in control and senescent AML12 cells. (**B**) Relative densitometric values of Western blots were calculated using ImageJ (NIH) software and normalized to GAPDH (n=3). (**C**) Western blot analysis of energy sensing and autophagic proteins including GAPDH in liver tissue from young and old mice. (**D**) Relative densitometric values of Western blots were calculated using ImageJ (NIH) software and normalized to GAPDH (n=5). (**E**) Western blot analysis of autophagy flux using lysosome inhibitor Bafilomycin A1 (Baf) in control and senescent AML12 cells under basal condition. (**F**) Relative densitometric values of Western blots were calculated using ImageJ (NIH) software and normalized to GAPDH (n=3). (**G**) Immunofluorescence analysis of neutral lipids accumulation (fat droplets) in control and senescent AML12 cells using BODIPY stain. Images were taken at 10x magnification. Control cells were treated overnight with 0.75 mM fatty acids Oleic Acid:Palmitic Acid (2:1) as a positive control. Scale bars as 100 mm. (**H**) Relative BODIPY fluorescence was calculated over Hoechst 33342 fluorescence using ImageJ software (NIH). (**I**) Hepatic triglyceride measurement was performed in the liver tissues from young and old mice. Statistical differences were calculated significant as *p<0.05 and ****p<0.0001.

hepatic aging *in vitro*. In particular, they showed increased expression of key senescence genes such as *Tp53*, *CDKN2A/p21*, and *CDKN1A/p16* as well as increased numbers of SA-βGal and γH2A.X positive cells that had condensed chromatin in larger nuclei (Figures 1 and 2).

Senescent cells are metabolically hyperactive and display a metabolic shift consisting of marked increases in glycolysis, mitochondrial activity, and mitochondrial damage due to proton leakage [8, 27, 28]. After AML12 cells were given multiple sublethal H_2O_2 doses, we found they increased their cellular bioenergetics (Figure 3A, 3B) and showed greater reliance upon glycolysis under nutrient stress conditions. Subsequent analysis of the glycolysis stress test confirmed senescent AML12 cells had greater glycolytic potential and reserve than control cells (Figure 3C, 3D). Senescent cells also have increased mitochondrial activity compared to control cells. However, this increased activity did not lead to more ATP production due to concomitant increases in basal uncoupling and proton leakage that occurred in senescent cells [1, 25]. These findings suggested that increased intracellular AMP:ATP concentration ratio in senescent cells may have led to the AMPK activation [1, 27, 29].

The senescent AML12 cells also had significantly higher basal respiration and maximum respiration than normal AML 12 cells (Figure 4A, 4B). However, these changes were not accompanied by increases in % spare respiratory capacity and ATP production. Notably, similar changes in mitochondrial function also have been reported to be present in livers from aged mice [1]. Previously, impairments in hepatic fatty acid oxidation and glucose intolerance have been described in the aged liver [1, 30]. In the senescent AML12 cells, mitochondrial fuel oxidation analysis also showed significantly lower fuel flexibility and less total capacity for glucose and fatty acid oxidation (Figure 4C). Taken together, our findings show that there is altered metabolism and mitochondrial function in senescent AML12 cells that resemble some of the changes previously reported in the aged liver [1, 8, 27, 28, 30].

Interestingly, senescent AML12 cells also showed a compensatory increase in mitochondrial glutamine oxidation (Figure 4C). Glutamine activates hepatic metabolic pathways involving PEPCK and the p70S6K. Phosphorylation of the latter enzymes leads to inhibition of autophagic proteolysis and induction of cell swelling [31, 32]. Glutamine oxidation also facilitates mTOR activation by leucine, an activator of

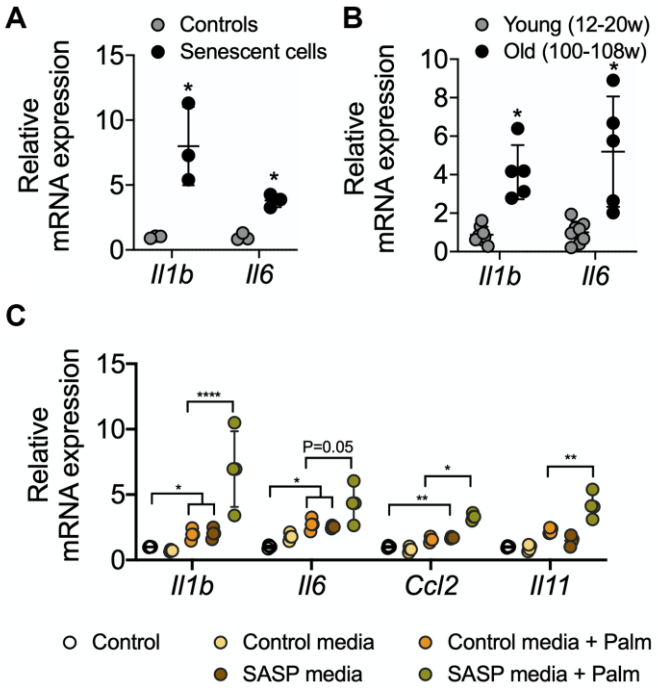

Figure 6. RT-qPCR analysis of SASP-related proinflammatory genes in senescent AML12 cells and liver tissues from young and old mice. RT-qPCR analysis of SASP-related proinflammatory genes in senescent AML12 cells (**A**) and liver tissues from young and old mice (**B**). (**C**) RT-qPCR analysis of inflammatory interleukins, chemokine CCL2 and fibrotic IL11 genes in control AML12 cells treated with conditional media from senescent AML12 cells (24 h) along with or without saturated fatty acids palmitate (0.5 mM for 24 h). Statistical differences were calculated significant as *p<0.05, **p<0.01, and ****p<0.0001.

glutaminolysis, to regulate cell growth and autophagy [33]. In this connection, we also observed decreased autophagy in senescent AML12 cells (Figure 5A, 5B). The activated mTOR signaling and increased p70S6K phosphorylation likely led to the inhibition of autophagy. Moreover, this decrease in autophagy and fatty acid oxidation likely contributed to the fuel-switching since we previously showed that both lipophagy and mitophagy are critical for β-oxidation of fatty acids in the liver [34–36]. Supporting this notion, we saw increased fat accumulation in the senescent cells (Figure 5E–5G). Our findings also were consistent with the observation that autophagy impairment associated with lysosomal and mitochondrial dysfunction is an important characteristic of oxidative stress-induced senescence [37]. On the other hand, our findings are in contrast to several studies that showed little or no change in autophagy during senescence in cells from other tissues [28, 38]. These differences suggest that there may be cell- and tissue-specific changes in autophagy during senescence occur. Nonetheless, it appears that in the liver, autophagy decreases with aging and may be involved in many age-related diseases such as NAFLD and Type 2 DM [1, 3, 11, 12, 39]. In this connection, we found that both senescent AML12 cells and livers from aged mice showed late autophagy block associated with increased intracellular fat content (Figure 5A–5G).

AMPK is a glucose and cellular energy sensor that is activated during states of energy depletion. In the liver, it can sense increased AMP:ATP and ADP:ATP concentration ratios, and activates compensatory responses such as increasing fatty acid oxidation, mitochondrial biogenesis, and glucose uptake, as well as inhibiting fatty acid synthesis [40, 41]. AMPK activation also induces cell cycle arrest and senescence by directly phosphorylating p53 at multiple sites [42]. In contrast to AMPK, which senses energy depletion and activates catabolic pathways, mTOR senses the fed state and activates anabolic pathways during cell growth and proliferation. Thus, AMPK and mTOR often have opposing roles in the metabolically active tissues of mammals [43]. However, the reciprocal actions of AMPK and mTOR that maintain metabolic homeostasis becomes impaired during senescence and leads to concurrent activation of both mTOR and AMPK. This dysregulation also is found in the aged liver [1, 27, 28]. Similarly, we found that both AMPK and mTOR were activated in senescent AML12 cells (Figure 5), suggesting that energy-sensing became dysregulated due to impaired oxidative phosphorylation, ATP production, (Figure 4A, 4B), and a compensatory increase in anaerobic glycolysis (Figure 3C, 3D).

Senescent cells employ an energy-dependent process to secrete SASP proteins comprised of high levels of inflammatory cytokines, immune modulators, growth factors, and proteases [7, 8, 28, 44, 45]. IL6 and IL1β are major secretory interleukins that are present in SASP proteins [1, 3, 8, 46]. In this connection, we observed that glycolysis increased in senescent AML12 cells (Figure 3C, 3D), and was accompanied by increased expression of IL6 and IL1β mRNA. Similar findings also were observed in livers from aged mice (Figure 6A, 6B). Interestingly, when we incubated healthy AML12 cells with conditional media collected from senescent AML12 cells, they became more sensitive to the inflammatory response caused by the saturated fatty acid, palmitate (Figure 6C). Our findings showed that SASP proteins play an important role in generating a pro-inflammatory environment during aging and age-related metabolic diseases, and were consistent with earlier reports on SASP proteins [1, 3, 8, 46].

In conclusion, we generated senescent AML12 hepatic cells that faithfully recapitulate many of the features of senescence found in livers of aged mice. In particular, the senescent AML12 cells expressed many of the key cellular markers of senescence and exhibited altered mitochondrial metabolism and molecular signaling that were similar to those found in the livers of aged mice. Most interestingly, they showed metabolic fuel switching from fatty acid utilization in normal AML12 cells to glycolysis and glutamine utilization. The increase in mTOR signaling, perhaps due to increased glycolysis, led to a decrease in autophagy which then decreased β-oxidation of fatty acids. This process further increased glycolysis and increased glutamine oxidation by the senescent AML12 cells. Furthermore, the senescent AML12 cells produced a pro-inflammatory environment that rendered neighboring hepatic cells more susceptible to saturated fatty acid-induced toxicity. The latter effect may occur in NAFLD during the progression from hepatosteatosis to non-alcoholic steatohepatitis (NASH). In summary, senescent AML 12 cells share many of the molecular, cell signaling, and metabolic characteristics found in the aged liver, and will be a useful tool for further mechanistic studies on aging in the liver.

MATERILS AND METHODS

Senescence induction in normal mouse AML12 cells and analysis of cell replication

The AML12 (alpha mouse liver 12) cells were purchased from ATCC, USA (ATCC® CRL-2254™) and maintained as described in the standard protocol (https://www.atcc.org/Products/All/CRL-2254.aspx#culturemethod). $4x10^6$ AML12 cells were seeded in a T175 cell culture flask for senescence induction. 30% (9.77 M) hydrogen peroxide (H_2O_2) was used for

senescence induction. At day 1, cells were treated with 1 mM H_2O_2 for 1 h in serum-free medium followed by incubation in complete DMEM:F12 medium (containing 10% FBS, 1x ITS, 100 nM dexamethasone, and 1x penicillin and streptomycin) for recovery for 23 h. from day 2 to day 6, 750 μM H_2O_2 for 1 h in serum-free medium followed by 23 h recovery was used. Morphological changes should be visualized from day 3 of H_2O_2 treatment (Figure 1B). At day 7, $0.3x10^6$ control and senescent AML12 cells were seeded in each well of 6-well plate for cell replication analysis and counted (using Countess™ II Automated Cell Counter, ThermoFisher) at every other day for three days as shown in Figure 1C.

Senescence-associated secretory phenotype (SASP) induced palmitate toxicity

AML12 senescence was induced as described above and after day 7 AML12 complete media was replaced with basal media (DMEM:F12) containing only 1x penicillin and streptomycin for 24 h. The next day, this conditional media was collected from control and senescent AML12 cells and put on new control AML12 cells seeded in other 6-well plates for 24 h. Palmitate was used at 0.5 mM concentration in 0.5% BSA supplemented (in a pathological FA:BSA ratio 6:1) in control media as well as senescent conditional media was used to represent pathological fatty acids concentration in serum [47]. Equivalent BSA was used as appropriate controls.

Animal experiments

12-20 weeks age male C57BL6/J mice (consider young), whereas 100-108 weeks age male C57BL6/J mice (consider old) were purchased from Jacksons Laboratory USA (Stock: 000664) and used in this study. Animals were housed in hanging polycarbonate cages under a 12 h light/12 h dark cycle at 23 °C with food and water available *ad libitum*. All cages contained shelters and nesting material. 6 h fasted mice were euthanized, and liver was collected and snap-frozen in liquid nitrogen for subsequent analysis. All mice were maintained according to the Guide for the Care and Use of Laboratory Animals (National Institutes of Health publication 1.0.0; revised 2011), and experiments were approved by SingHealth Institutional Animal Care and Use Committee.

mRNA expression analysis by reverse transcription-quantitative PCR

Total RNA isolation from cultured cells and liver tissue was performed using InviTrap Spin Universal RNA kit (Stratec Biomedical, Birkenfeld, Germany), and RT-qPCR was performed as described previously [48] using QuantiTect SYBR Green PCR kit and KiCqStart SYBR Green optimized primers from Sigma-Aldrich (KSPQ12012).

Protein extraction and expression analysis by Western blotting

Cultured cells or 50 mg of liver tissues were lysed using CelLytic M mammalian cell lysis/extraction reagent (C2978, Sigma-Aldrich). An aliquot was removed, and protein concentrations were measured using the BCA kit (Bio-Rad). Western blotting was performed using a standard protocol, as described previously [49]. Primary antibodies at dilution 1:500 for phospho-AMPK-alpha (T172) (CST: 2535S), AMPK-alpha (D5A2) (CST: 5831S), phospho-AKT (S473) (CST: 4058S), AKT (CST: 9272S), phospho-mTOR (S2448) (CST: 5536S), mTOR (7C10) (CST: 2983S), phospho-p70S6K (Thr389) (CST: 9206S), p70S6K (CST: 9202s) 1:5000 for LC3B-II (CST: 2775S), GAPDH (CST: 2118L), and 1:1000 for p62 (CST: 5114S) were used. Western blot images were captured on the Gel-Doc system (Bio-Rad), and densitometry analysis was performed using ImageJ software (National Institutes of Health). The integrated density of the target protein was normalized with the GAPDH; the mean was plotted in graphs.

Immunofluorescence analysis for γH2A.X

Cells were cultured in 4-well chambered slides, fixed in 4% paraformaldehyde and incubated in 1:200 diluted γH2A.X antibody (CST: 9718) overnight at 4 ^oC after blocking as described previously [36]. 1:200 Alexa Fluor 488 (Molecular Probes, ThermoFisher) was used to collect signals. Cells were counter-stained with 5 μM Hoechst 33342 (Abcam: ab228551) for 5 min and mounted using VECTASHIELD® Antifade Mounting Medium H-1000 (Vector Laboratories) and visualized under 40x magnification using Zeiss LSM confocal microscope. Five images were clicked randomly using ZEN 2 (blue edition) software and quantification of green fluorescence was normalized with blue using ImageJ software (National Institutes of Health) and plotted as a graph.

Senescent associated β-Gal staining in AML12 cells

Cellular Senescence Assay kit (Merck Millipore: KAA002) was used to detect senescent AML12 by SA β-Gal staining as per the manufacturer's protocol. X-Gal staining was performed overnight at 37 ^0C and crystals were visualized under the microscope at 10x magnification. Five images were captured randomly using an Olympus inverted microscope and cells were counted for SA β-Gal^+ Cells, and shown as percent positive cells.

Seahorse extracellular flux analysis for bioenergetic phenotyping, mitostress test, glycolytic stress test and mitochondrial fuel oxidation analysis

Seahorse extracellular flux analyser XFe96 (Agilent) was used for bioenergetic phenotyping, mitostress test, glycolytic stress test and mitochondrial fuel oxidation analysis, and Seahorse Wave Desktop software was used for report generation and data analysis, and GraphPad PRISM 8 was used for statistical analysis and data presentation.

Bioenergetic phenotyping: Agilent Seahorse XF Cell Energy Phenotype Test kit was used with Agilent Seahorse XFe96 Extracellular Flux Analyzer that rapidly measures mitochondrial respiration and glycolysis under baseline and stressed conditions, to reveal the three key parameters of cell energy metabolism: Baseline Phenotype, Stressed Phenotype, and Metabolic Potential (https://www.agilent.com/cs/library/usermanuals/public/XF_Cell_Energy_Phenotype_Test_Kit_User_Guide.pdf). Simultaneous acute injections of mitochondrial inhibitors oligomycin and FCCP reveals live cell's metabolic potential under stress. Oligomycin (1 μM) inhibits ATP production by the mitochondria, and causes a compensatory increase in the rate of glycolysis as the cells attempt to meet their energy demands via the glycolytic pathway. Whereas, FCCP (1 μM) depolarizes the mitochondrial membrane, and drives oxygen consumption rates higher as the mitochondria attempt to restore the mitochondrial membrane potential.

Glycolysis stress test: Agilent Seahorse XF Glycolysis Stress Test Kit was used as per the standard protocol by Agilent Seahorse (https://www.agilent.com/en-us/agilent404?s=www.agilent.com/cs/library/usermanuals/public/XF_Glycolysis_Stress_Test_Kit_User_Guide.pdf). Glucose conversion to lactate (Glycolysis) results in net production and extrusion of protons into the extracellular medium (acidification). As glycolysis occurs, the resulting acidification of the medium surrounding the cells is measured directly by the analyzer and reported as the Extracellular Acidification Rate (ECAR).

To understand the complete glycolytic potential of the cell, ECAR of cells was measured (three times) before and after sequential injections of three different compounds, glucose (10 mM), oligomycin (1 μM) and 2-Deoxy-D-glucose (2-DG; 100 mM) sequentially.

Mito stress test: Agilent Seahorse XF Mito Stress Test Kit was used as per the standard protocol by Agilent Seahorse (https://www.agilent.com/cs/library/usermanuals/public/XF_Cell_Mito_Stress_Test_Kit_User_Guide.pdf). This test measures key parameters of mitochondrial function by directly measuring the oxygen consumption rate (OCR) of cells. Oligomycin (1 μM; inhibits ATP synthase) was injected first following basal OCR measurements. The second injection of FCCP (1 μM; an uncoupling agent that collapses the proton gradient and disrupts the mitochondrial membrane potential) followed by the third injection which was a mixture of rotenone (1 μM; a complex I inhibitor) and antimycin A (1 μM; a complex III inhibitor).

Mito fuel flex test: Agilent Seahorse XF Mito Fuel Flex Test Kit was used as per the standard protocol by Agilent Seahorse (https://www.agilent.com/cs/library/usermanuals/public/XF_Mito_Fuel_Flex_Test_Kit_User_Guide%20old.pdf). This test measures the dependency, capacity, and flexibility of cells to oxidize three mitochondrial fuels in real-time in living cells: Glucose (pyruvate), Glutamine (glutamate) and Long-chain fatty acids. This test determines the rate of oxidation of each of these fuels by measuring OCR of cells in the presence or absence of fuel pathway inhibitors. UK5099 (2 μM; glucose oxidation pathway inhibitor) that blocks the mitochondrial pyruvate carrier (MPC); BPTES (3 μM; glutamine oxidation pathway inhibitor) that allosterically inhibits glutaminase (GLS1); and Etomoxir (4 μM; long-chain fatty acid oxidation inhibitor) that inhibits carnitine palmitoyl-transferase 1A (CPT1A), a critical enzyme of mitochondrial beta-oxidation.

The data later represented as fuel oxidation dependency, flexibility and total capacity. 'Dependency' indicates the fuel oxidation at basal in control or senescence cells. Inhibiting the two alternative pathways followed by the pathway of interest enables the calculation of cells' mitochondrial 'capacity' to meet energy demand. 'Flexibility' (that is calculated by subtracting the dependency from the capacity for the target fuel oxidation pathway) indicates the cells' mitochondria can compensate for the inhibited pathway by using other pathways to fuel mitochondrial respiration. The presence of dependency and the absence of flexibility demonstrates that the mitochondria require that fuel pathway to maintain basal OCR.

Immunofluorescence imaging of intracellular lipids using BODIPY™ 493/503

Control and senescent AML12 cells were seeded in 24-well plate at 7th day of the protocol, and cultured for 24 h. Cells were rinsed with 1x PBS and stained with BODIPY™ 493/503 (D3922; Molecular Probes, ThermoFisher Scientific) at 1:1000 dilution for 15 min. Cells were then rinsed with 1xPBS containing Hoechst 33342 (Sigma) to counterstain nucleus for 5 min. After the rinse, cells were kept in 1x HBSS for imaging. Leica fluorescent microscope was used at 10x magnification for

visualization and LAS X imaging software was used for image capture.

Liver triglycerides measurements in young and old mice

Liver triglyceride was measured using triglyceride colorimetric assay kit (Cayman Chemical) as per the manufacturer's protocol.

RNAseq and pathway analysis

We performed RNAseq analysis on three polled samples of each control and senescent AML12 cells to understand the pathways regulated during senescence induction. The RNAseq dataset is submitted as Series record GSE151806 on Gene Expression Omnibus, NCBI. The detailed method on RNAseq analysis is provided as supplementary methods. Significant ($p<0.05$) deferentially expressed genes with threshold more than 1.5 log2fold change or less than -1.5 log2fold change were analyzed for upregulated or downregulated pathway using EnrichR online pathway analysis platform (https://amp.pharm.mssm.edu/Enrichr/) [50, 51]. Pathways were captured from KEGG 2019 Human, Reactome 2016, as well as Gene Ontology (GO) biological process and molecular functions databases.

Statistical methods

The data was calculated and presented as Mean±SD. The parametric unpaired t-test was used to compute significance between two groups, whereas Two-way ANOVA followed by Tukey's multiple comparisons test was used to compute significance between more than two groups. GraphPad PRISM 8 was used for statistical analysis and data representation.

AUTHOR CONTRIBUTIONS

Conceived and designed the experiments: BKS MT. Performed the experiments: BKS MT RS KT. Analyzed the data: BKS MT JZ. Contributed reagents/materials /analysis tools: PMY BKS MT JZ. Wrote the manuscript: BKS MT PMY.

ACKNOWLEDGMENTS

The authors would like to thank Ms. Jia Pei and Mr. Kiraely Adam Wong Zongren for their assistance and help during this study. The authors also like to thank NovogeneAIT for providing RNAseq services.

CONFLICTS OF INTEREST

The authors declare no conflicts of interest.

FUNDING

This research was funded by the Ministry of Health (MOH), and National Medical Research Council (NMRC), Singapore, grant number NMRC/OFYIRG/0002/2016 and MOH-000319 (MOH-OFIRG19may-0002) to BKS; NMRC/OFYIRG/077/2018 to MT; and CSAI19may-0002 to PMY; Duke-NUS Medical School and Estate of Tan Sri Khoo Teck Puat Khoo Pilot Award (Collaborative) Duke-NUS-KP(Coll)/2018/0007A to JZ.

REFERENCES

1. Hunt NJ, Kang SW, Lockwood GP, Le Couteur DG, Cogger VC. Hallmarks of aging in the liver. Comput Struct Biotechnol J. 2019; 17:1151–61. https://doi.org/10.1016/j.csbj.2019.07.021 PMID:31462971

2. Jiang JX, Fish SR, Tomilov A, Li Y, Fan W, Dehnad A, Gae D, Das S, Mozes G, Charville GW, Ramsey J, Cortopassi G, Török NJ. Non-phagocytic activation of NOX2 is implicated in progressive non-alcoholic steatohepatitis during aging. Hepatology. 2020. [Epub ahead of print]. https://doi.org/10.1002/hep.31118 PMID:31950520

3. Kim IH, Kisseleva T, Brenner DA. Aging and liver disease. Curr Opin Gastroenterol. 2015; 31:184–91. https://doi.org/10.1097/MOG.0000000000000176 PMID:25850346

4. Papatheodoridi AM, Chrysavgis L, Koutsilieris M, Chatzigeorgiou A. The role of senescence in the development of nonalcoholic fatty liver disease and progression to nonalcoholic steatohepatitis. Hepatology. 2020; 71:363–74. https://doi.org/10.1002/hep.30834 PMID:31230380

5. Campisi J, Kapahi P, Lithgow GJ, Melov S, Newman JC, Verdin E. From discoveries in ageing research to therapeutics for healthy ageing. Nature. 2019; 571:183–92. https://doi.org/10.1038/s41586-019-1365-2 PMID:31292558

6. Ferrucci L, Gonzalez-Freire M, Fabbri E, Simonsick E, Tanaka T, Moore Z, Salimi S, Sierra F, de Cabo R. Measuring biological aging in humans: a quest. Aging Cell. 2020; 19:e13080. https://doi.org/10.1111/acel.13080 PMID:31833194

7. Gorgoulis V, Adams PD, Alimonti A, Bennett DC, Bischof O, Bishop C, Campisi J, Collado M, Evangelou K, Ferbeyre G, Gil J, Hara E, Krizhanovsky V, et al. Cellular senescence: defining a path forward. Cell. 2019; 179:813–27.

https://doi.org/10.1016/j.cell.2019.10.005
PMID:31675495

8. Hernandez-Segura A, Nehme J, Demaria M. Hallmarks of cellular senescence. Trends Cell Biol. 2018; 28:436–53. https://doi.org/10.1016/j.tcb.2018.02.001 PMID:29477613

9. Schmeer C, Kretz A, Wengerodt D, Stojiljkovic M, Witte OW. Dissecting aging and senescence-current concepts and open lessons. Cells. 2019; 8:1446. https://doi.org/10.3390/cells8111446 PMID:31731770

10. Stahl EC, Haschak MJ, Popovic B, Brown BN. Macrophages in the aging liver and age-related liver disease. Front Immunol. 2018; 9:2795. https://doi.org/10.3389/fimmu.2018.02795 PMID:30555477

11. Baker BM, Haynes CM. Mitochondrial protein quality control during biogenesis and aging. Trends Biochem Sci. 2011; 36:254–61. https://doi.org/10.1016/j.tibs.2011.01.004 PMID:21353780

12. Belikov AV. Age-related diseases as vicious cycles. Ageing Res Rev. 2019; 49:11–26. https://doi.org/10.1016/j.arr.2018.11.002 PMID:30458244

13. Palmer AK, Gustafson B, Kirkland JL, Smith U. Cellular senescence: at the nexus between ageing and diabetes. Diabetologia. 2019; 62:1835–41. https://doi.org/10.1007/s00125-019-4934-x PMID:31451866

14. Palmer AK, Xu M, Zhu Y, Pirtskhalava T, Weivoda MM, Hachfeld CM, Prata LG, van Dijk TH, Verkade E, Casaclang-Verzosa G, Johnson KO, Cubro H, Doornebal EJ, et al. Targeting senescent cells alleviates obesity-induced metabolic dysfunction. Aging Cell. 2019; 18:e12950. https://doi.org/10.1111/acel.12950 PMID:30907060

15. Patil P, Dong Q, Wang D, Chang J, Wiley C, Demaria M, Lee J, Kang J, Niedernhofer LJ, Robbins PD, Sowa G, Campisi J, Zhou D, Vo N. Systemic clearance of $p16^{INK4a}$-positive senescent cells mitigates age-associated intervertebral disc degeneration. Aging Cell. 2019; 18:e12927. https://doi.org/10.1111/acel.12927 PMID:30900385

16. Thoppil H, Riabowol K. Senolytics: a translational bridge between cellular senescence and organismal aging. Front Cell Dev Biol. 2020; 7:367. https://doi.org/10.3389/fcell.2019.00367 PMID:32039197

17. Ogrodnik M, Miwa S, Tchkonia T, Tiniakos D, Wilson CL, Lahat A, Day CP, Burt A, Palmer A, Anstee QM, Grellscheid SN, Hoeijmakers JH, Barnhoorn S, et al. Cellular senescence drives age-dependent hepatic steatosis. Nat Commun. 2017; 8:15691. https://doi.org/10.1038/ncomms15691 PMID:28608850

18. Chen JH, Ozanne SE, Hales CN. Methods of cellular senescence induction using oxidative stress. Methods Mol Biol. 2007; 371:179–89. https://doi.org/10.1007/978-1-59745-361-5_14 PMID:17634582

19. Carnero A. Markers of cellular senescence. Methods Mol Biol. 2013; 965:63–81. https://doi.org/10.1007/978-1-62703-239-1_4 PMID:23296651

20. Chen H, Li Y, Tollefsbol TO. Cell senescence culturing methods. Methods Mol Biol. 2013; 1048:1–10. https://doi.org/10.1007/978-1-62703-556-9_1 PMID:23929093

21. Aravinthan A, Shannon N, Heaney J, Hoare M, Marshall A, Alexander GJ. The senescent hepatocyte gene signature in chronic liver disease. Exp Gerontol. 2014; 60:37–45. https://doi.org/10.1016/j.exger.2014.09.011 PMID:25240687

22. Pan C, Lang H, Zhang T, Wang R, Lin X, Shi P, Zhao F, Pang X. Conditioned medium derived from human amniotic stem cells delays H2O2-induced premature senescence in human dermal fibroblasts. Int J Mol Med. 2019; 44:1629–40. https://doi.org/10.3892/ijmm.2019.4346 PMID:31545472

23. Childs BG, Gluscevic M, Baker DJ, Laberge RM, Marquess D, Dananberg J, van Deursen JM. Senescent cells: an emerging target for diseases of ageing. Nat Rev Drug Discov. 2017; 16:718–35. https://doi.org/10.1038/nrd.2017.116 PMID:28729727

24. Liguori I, Russo G, Curcio F, Bulli G, Aran L, Della-Morte D, Gargiulo G, Testa G, Cacciatore F, Bonaduce D, Abete P. Oxidative stress, aging, and diseases. Clin Interv Aging. 2018; 13:757–72. https://doi.org/10.2147/CIA.S158513 PMID:29731617

25. Panel M, Ghaleb B, Morin D. Mitochondria and aging: a role for the mitochondrial transition pore? Aging Cell. 2018; 17:e12793. https://doi.org/10.1111/acel.12793 PMID:29888494

26. Coppé JP, Patil CK, Rodier F, Sun Y, Muñoz DP, Goldstein J, Nelson PS, Desprez PY, Campisi J.

Senescence-associated secretory phenotypes reveal cell-nonautonomous functions of oncogenic RAS and the p53 tumor suppressor. PLoS Biol. 2008; 6:2853–68. https://doi.org/10.1371/journal.pbio.0060301 PMID:19053174

27. Sabbatinelli J, Prattichizzo F, Olivieri F, Procopio AD, Rippo MR, Giuliani A. Where metabolism meets senescence: focus on endothelial cells. Front Physiol. 2019; 10:1523. https://doi.org/10.3389/fphys.2019.01523 PMID:31920721

28. Wiley CD, Campisi J. From ancient pathways to aging cells-connecting metabolism and cellular senescence. Cell Metab. 2016; 23:1013–21. https://doi.org/10.1016/j.cmet.2016.05.010 PMID:27304503

29. Stead ER, Castillo-Quan JI, Miguel VE, Lujan C, Ketteler R, Kinghorn KJ, Bjedov I. Agephagy - adapting autophagy for health during aging. Front Cell Dev Biol. 2019; 7:308. https://doi.org/10.3389/fcell.2019.00308 PMID:31850344

30. Gong Z, Tas E, Yakar S, Muzumdar R. Hepatic lipid metabolism and non-alcoholic fatty liver disease in aging. Mol Cell Endocrinol. 2017; 455:115–30. https://doi.org/10.1016/j.mce.2016.12.022 PMID:28017785

31. Meynial-Denis D. Glutamine metabolism in advanced age. Nutr Rev. 2016; 74:225–36. https://doi.org/10.1093/nutrit/nuv052 PMID:26936258

32. Häussinger D, Schliess F. Glutamine metabolism and signaling in the liver. Front Biosci. 2007; 12:371–91. https://doi.org/10.2741/2070 PMID:17127305

33. Durán RV, Oppliger W, Robitaille AM, Heiserich L, Skendaj R, Gottlieb E, Hall MN. Glutaminolysis activates rag-mTORC1 signaling. Mol Cell. 2012; 47:349–58. https://doi.org/10.1016/j.molcel.2012.05.043 PMID:22749528

34. Sinha RA, Singh BK, Zhou J, Wu Y, Farah BL, Ohba K, Lesmana R, Gooding J, Bay BH, Yen PM. Thyroid hormone induction of mitochondrial activity is coupled to mitophagy via ROS-AMPK-ULK1 signaling. Autophagy. 2015; 11:1341–57. https://doi.org/10.1080/15548627.2015.1061849 PMID:26103054

35. Sinha RA, Farah BL, Singh BK, Siddique MM, Li Y, Wu Y, Ilkayeva OR, Gooding J, Ching J, Zhou J, Martinez L, Xie S, Bay BH, et al. Caffeine stimulates hepatic lipid metabolism by the autophagy-lysosomal pathway in mice. Hepatology. 2014; 59:1366–80. https://doi.org/10.1002/hep.26667 PMID:23929677

36. Singh BK, Sinha RA, Tripathi M, Mendoza A, Ohba K, Sy JA, Xie SY, Zhou J, Ho JP, Chang CY, Wu Y, Giguère V, Bay BH, et al. Thyroid hormone receptor and ERRα coordinately regulate mitochondrial fission, mitophagy, biogenesis, and function. Sci Signal. 2018; 11:eaam5855. https://doi.org/10.1126/scisignal.aam5855 PMID:29945885

37. Tai H, Wang Z, Gong H, Han X, Zhou J, Wang X, Wei X, Ding Y, Huang N, Qin J, Zhang J, Wang S, Gao F, et al. Autophagy impairment with lysosomal and mitochondrial dysfunction is an important characteristic of oxidative stress-induced senescence. Autophagy. 2017; 13:99–113. https://doi.org/10.1080/15548627.2016.1247143 PMID:27791464

38. Cho S, Hwang ES. Status of mTOR activity may phenotypically differentiate senescence and quiescence. Mol Cells. 2012; 33:597–604. https://doi.org/10.1007/s10059-012-0042-1 PMID:22570149

39. Amir M, Czaja MJ. Autophagy in nonalcoholic steatohepatitis. Expert Rev Gastroenterol Hepatol. 2011; 5:159–66. https://doi.org/10.1586/egh.11.4 PMID:21476911

40. Hardie DG, Ross FA, Hawley SA. AMPK: a nutrient and energy sensor that maintains energy homeostasis. Nat Rev Mol Cell Biol. 2012; 13:251–62. https://doi.org/10.1038/nrm3311 PMID:22436748

41. Lin SC, Hardie DG. AMPK: sensing glucose as well as cellular energy status. Cell Metab. 2018; 27:299–313. https://doi.org/10.1016/j.cmet.2017.10.009 PMID:29153408

42. Jones RG, Plas DR, Kubek S, Buzzai M, Mu J, Xu Y, Birnbaum MJ, Thompson CB. AMP-activated protein kinase induces a p53-dependent metabolic checkpoint. Mol Cell. 2005; 18:283–93. https://doi.org/10.1016/j.molcel.2005.03.027 PMID:15866171

43. Gwinn DM, Shaw RJ. (2010). AMPK Control of mTOR Signaling and Growth. In: Tamanoi F, Hall MN, eds. The Enzymes: Elsevier, v.28: pp. 49–75. https://doi.org/10.1016/S1874-6047(10)28003-4

44. Herranz N, Gil J. Mechanisms and functions of cellular senescence. J Clin Invest. 2018; 128:1238–46. https://doi.org/10.1172/JCI95148 PMID:29608137

45. Tchkonia T, Zhu Y, van Deursen J, Campisi J, Kirkland JL. Cellular senescence and the senescent secretory phenotype: therapeutic opportunities. J Clin Invest. 2013; 123:966–72. https://doi.org/10.1172/JCI64098 PMID:23454759

46. Chen H, Ruiz PD, McKimpson WM, Novikov L, Kitsis RN, Gamble MJ. MacroH2A1 and ATM play opposing roles in paracrine senescence and the senescence-associated secretory phenotype. Mol Cell. 2015; 59:719–31. https://doi.org/10.1016/j.molcel.2015.07.011 PMID:26300260

47. Alsabeeh N, Chausse B, Kakimoto PA, Kowaltowski AJ, Shirihai O. Cell culture models of fatty acid overload: problems and solutions. Biochim Biophys Acta Mol Cell Biol Lipids. 2018; 1863:143–51. https://doi.org/10.1016/j.bbalip.2017.11.006 PMID:29155055

48. Zhou J, Chong SY, Lim A, Singh BK, Sinha RA, Salmon AB, Yen PM. Changes in macroautophagy, chaperone-mediated autophagy, and mitochondrial metabolism in murine skeletal and cardiac muscle during aging. Aging (Albany NY). 2017; 9:583–99. https://doi.org/10.18632/aging.101181 PMID:28238968

49. Singh BK, Sinha RA, Zhou J, Tripathi M, Ohba K, Wang ME, Astapova I, Ghosh S, Hollenberg AN, Gauthier K, Yen PM. Hepatic FOXO1 target genes are co-regulated by thyroid hormone via RICTOR protein deacetylation and MTORC2-AKT protein inhibition. J Biol Chem. 2016; 291:198–214. https://doi.org/10.1074/jbc.M115.668673 PMID:26453307

50. Kuleshov MV, Jones MR, Rouillard AD, Fernandez NF, Duan Q, Wang Z, Koplev S, Jenkins SL, Jagodnik KM, Lachmann A, McDermott MG, Monteiro CD, Gundersen GW, Ma'ayan A. Enrichr: a comprehensive gene set enrichment analysis web server 2016 update. Nucleic Acids Res. 2016; 44:W90–97. https://doi.org/10.1093/nar/gkw377 PMID:27141961

51. Chen EY, Tan CM, Kou Y, Duan Q, Wang Z, Meirelles GV, Clark NR, Ma'ayan A. Enrichr: interactive and collaborative HTML5 gene list enrichment analysis tool. BMC Bioinformatics. 2013; 14:128. https://doi.org/10.1186/1471-2105-14-128 PMID:23586463

SUPPLEMENTARY MATERIALS

RNAseq

Data analysis

Downstream analysis was performed using a combination of programs including STAR, HTseq, Cufflink and our wrapped scripts. Alignments were parsed using Tophat program and differential expressions were determined through DESeq2/edgeR. GO and KEGG enrichment were implemented by the ClusterProfiler. Gene fusion and difference of alternative splicing event were detected by Star-fusion and rMATS software

Reads mapping to the reference genome

Reference genome and gene model annotation files were downloaded from genome website browser (NCBI/UCSC/Ensembl) directly. Indexes of the reference genome was built using STAR and paired-end clean reads were aligned to the reference genome using STAR (v2.5) [1]. STAR used the method of Maximal Mappable Prefix(MMP) which can generate a precise mapping result for junction reads.

Quantification of gene expression level

HTSeq v0.6.1 was used to count the read numbers mapped of each gene. And then FPKM of each gene was calculated based on the length of the gene and reads count mapped to this gene. FPKM, Reads Per Kilobase of exon model per Million mapped reads, considers the effect of sequencing depth and gene length for the reads count at the same time, and is currently the most commonly used method for estimating gene expression levels [2].

Differential expression analysis

(For DESeq2 with biological replicates) Differential expression analysis between two conditions/groups (two biological replicates per condition) was performed using the DESeq2 R package (2_1.6.3). DESeq2 provide statistical routines for determining differential expression in digital gene expression data using a model based on the negative binomial distribution. The resulting P-values were adjusted using the Benjamini and Hochberg's approach for controlling the False Discovery Rate(FDR) [3]. Genes with an adjusted P-value <0.05 found by DESeq2 were assigned as differentially expressed [4].

(For edgeR without biological replicates) Prior to differential gene expression analysis, for each sequenced library, the read counts were adjusted by edgeR program package through one scaling normalized factor. Differential expression analysis of two conditions was performed using the edgeR R package (3.16.5). The P values were adjusted using the Benjamini & Hochberg method. Corrected P-value of 0.05 and absolute foldchange of 1 were set as the threshold for significantly differential expression [5].

The Venn diagrams were prepared using the function venn Diagram in R based on the gene list for different group.

Correlations

To allow for log adjustment, genes with 0 FPKM are assigned a value of 0.001. Correlation were determined using the cor.test function in R with options set alternative ="greater" and method = "Spearman".

Clustering

To identify the correlation between difference, we clustered different samples using expression level FPKM to see the correlation using hierarchical clustering distance method with the function of heatmap, SOM(Self-organization mapping) and kmeans using silhouette coefficient to adapt the optimal classification with default parameter in R.

GO and KEGG enrichment analysis of differentially expressed genes

Gene Ontology (GO) enrichment analysis of differentially expressed genes was implemented by the clusterProfiler R package, in which gene length bias was corrected. GO terms with corrected P value less than 0.05 were considered significantly enriched by differential expressed genes [6].

KEGG [7] is a database resource for understanding high-level functions and utilities of the biological system, such as the cell, the organism and the ecosystem, from molecular level information, especially large-scale molecular datasets generated by genome sequencing and other high-through put experimental technologies (http://www.genome.jp/kegg/). We used clusterProfiler R package to test the statistical enrichment of differential expression genes in KEGG pathways.

PPI analysis of differentially expressed genes

PPI analysis of differentially expressed genes was based on the STRING database, which contained known and predicted Protein-Protein Interactions. For the species existing in the database(like human and mouse), we

constructed the networks by extracting the target gene lists from the database [8].

Fusion gene analysis

Fusion gene is refers to the two genes of all or part of the sequences perform fusion ,results of the chimeric gene, usually caused by reasons such as chromosome translocation and problem. We used Star-fusion(0.8.0) software analysis and detection of fusion genes [9].

Alternative splicing analysis

Alternative Splicing is an important mechanism for regulate the expression of genes and the variable of protein. rMATS(3.2.1) software was used to analysis the ASevent [6].

SNP analysis

We deal with the bam alignment results of each sample by using picard tools(v1.111) and samtools(v0.1.18), including reorder, sort, add head information, mark duplicates, local realignment around indels and base qulaity score recalibration [10]. Then we call snp by the tool HaplotypeCaller in GATK3.4 version [11]. Finally, we ues annovar to do SNP annotation against dbSNP database and some other database.

Differentially expressed gene annotation

TFCat and Cosmic database were used to annotate the differential expressed gene. TFCat is a curated catalogue of mouse and human transcription factors (TF) based on a reliable core collection of annotations obtained by expert review of the scientific literature [12]. COSMIC is a database designed to store and display somatic mutation information and related details which contains information relating to human cancers.

Data access

The high-throughput sequencing data from this study have been submitted to the GEO-NCBI under accession number GSE151806.

ACKNOWLEDGMENTS

We thank NovogeneAIT for technical supports and deep discussion.

REFERENCES

1. Dobin A, Davis CA, Schlesinger F, Drenkow J, Zaleski C, Jha S, Batut P, Chaisson M, Gingeras TR. STAR: ultrafast universal RNA-seq aligner. Bioinformatics. 2013; 29:15–21. https://doi.org/10.1093/bioinformatics/bts635 PMID:23104886

2. Mortazavi A, Williams BA, McCue K, Schaeffer L, Wold B. Mapping and quantifying mammalian transcriptomes by RNA-seq. Nat Methods. 2008; 5:621–28. https://doi.org/10.1038/nmeth.1226 PMID:18516045

3. Dillies MA, Rau A, Aubert J, Hennequet-Antier C, Jeanmougin M, Servant N, Keime C, Marot G, Castel D, Estelle J, Guernec G, Jagla B, Jouneau L, et al, and French StatOmique Consortium. A comprehensive evaluation of normalization methods for illumina high-throughput RNA sequencing data analysis. Brief Bioinform. 2013; 14:671–83. https://doi.org/10.1093/bib/bbs046 PMID:22988256

4. Anders S, Huber W. Differential expression analysis for sequence count data. Genome Biol. 2010; 11:R106. https://doi.org/10.1186/gb-2010-11-10-r106 PMID:20979621

5. Robinson MD, McCarthy DJ, Smyth GK. edgeR: a bioconductor package for differential expression analysis of digital gene expression data. Bioinformatics. 2010; 26:139–40. https://doi.org/10.1093/bioinformatics/btp616 PMID:19910308

6. Shen S, Park JW, Lu ZX, Lin L, Henry MD, Wu YN, Zhou Q, Xing Y. rMATS: robust and flexible detection of differential alternative splicing from replicate RNA-seq data. Proc Natl Acad Sci USA. 2014; 111:E5593–601. https://doi.org/10.1073/pnas.1419161111 PMID:25480548

7. Ogata H, Goto S, Sato K, Fujibuchi W, Bono H, Kanehisa M. KEGG: kyoto encyclopedia of genes and genomes. Nucleic Acids Res. 1999; 27:29–34. https://doi.org/10.1093/nar/27.1.29 PMID:9847135

8. Shannon P, Markiel A, Ozier O, Baliga NS, Wang JT, Ramage D, Amin N, Schwikowski B, Ideker T. Cytoscape: a software environment for integrated models of biomolecular interaction networks. Genome Res. 2003; 13:2498–504. https://doi.org/10.1101/gr.1239303 PMID:14597658

9. Haas BJ, Dobin A, Stransky N, Li B, Yang X, Tickle T, Bankapur A, Ganote C, Doak TG, Pochet N, Sun J, Wu CJ, Gingeras TR, et al. STAR-Fusion: Fast and Accurate Fusion Transcript Detection from RNA-Seq. bioRxiv. 2017. https://doi.org/10.1101/120295

10. Chepelev I, Wei G, Tang Q, Zhao K. Detection of single nucleotide variations in expressed exons of the human

genome using RNA-seq. Nucleic Acids Res. 2009; 37:e106. https://doi.org/10.1093/nar/gkp507 PMID:19528076

11. McKenna A, Hanna M, Banks E, Sivachenko A, Cibulskis K, Kernytsky A, Garimella K, Altshuler D, Gabriel S, Daly M, DePristo MA. The genome analysis toolkit: a MapReduce framework for analyzing next-generation DNA sequencing data. Genome Res. 2010; 20:1297–303. https://doi.org/10.1101/gr.107524.110 PMID:20644199

12. Fulton DL, Sundararajan S, Badis G, Hughes TR, Wasserman WW, Roach JC, Sladek R. TFCat: the curated catalog of mouse and human transcription factors. Genome Biol. 2009; 10:R29. https://doi.org/10.1186/gb-2009-10-3-r29 PMID:19284633

Supplementary Figures

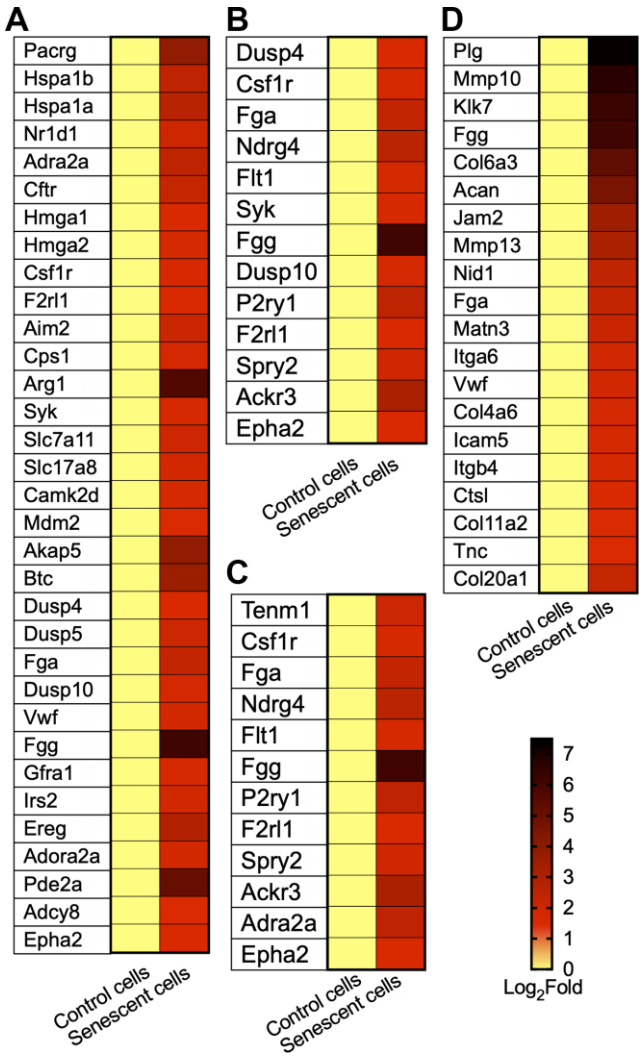

Supplemenatry Figure 1. RNAseq analysis of control and senescent AML12 cells for upregulated pathways. (**A**) Heat map showing genes regulating pathways: cAMP metabolic process (GO:0046058), positive regulation of tumor necrosis factor-mediated signaling pathway (GO:1903265), cellular response to unfolded protein (GO:0034620), regulation of insulin secretion involved in cellular response to glucose stimulus (GO:0061178), positive regulation of cellular senescence (GO:2000774), positive regulation of cell aging (GO:0090343), regulation of chemokine secretion (GO:0090196), interleukin-1 beta secretion (GO:0050702), interleukin-1 beta production (GO:0032611), bile acid biosynthetic process (GO:0006699), urea cycle (GO:0000050), regulation of superoxide anion generation (GO:0032928), L-glutamate transmembrane transporter activity (GO:0005313), Glutamate Binding, Activation of AMPA Receptors and Synaptic Plasticity Homo sapiens R-HSA-399721, Insulin receptor signalling cascade Homo sapiens R-HSA-74751, Signaling by Type 1 Insulin-like Growth Factor 1 Receptor (IGF1R) Homo sapiens R-HSA-2404192, IRS-mediated signalling Homo sapiens R-HSA-112399, and Signaling by Insulin receptor Homo sapiens R-HSA-74752. (**B**) Heat map showing genes regulating pathways: regulation of ERK1 and ERK2 cascade (GO:0070372), and Prolonged ERK activation events Homo sapiens R-HSA-169893. (**C**) Heat map showing genes regulating pathway: positive regulation of MAPK cascade (GO:0043410). (**D**) Heat map showing genes regulating pathway: interleukin-1 beta secretion (GO:0050702), interleukin-1 beta production (GO:0032611), extracellular matrix organization (GO:0030198), ECM-receptor interaction; Extracellular matrix organization Homo sapiens R-HSA-1474244.

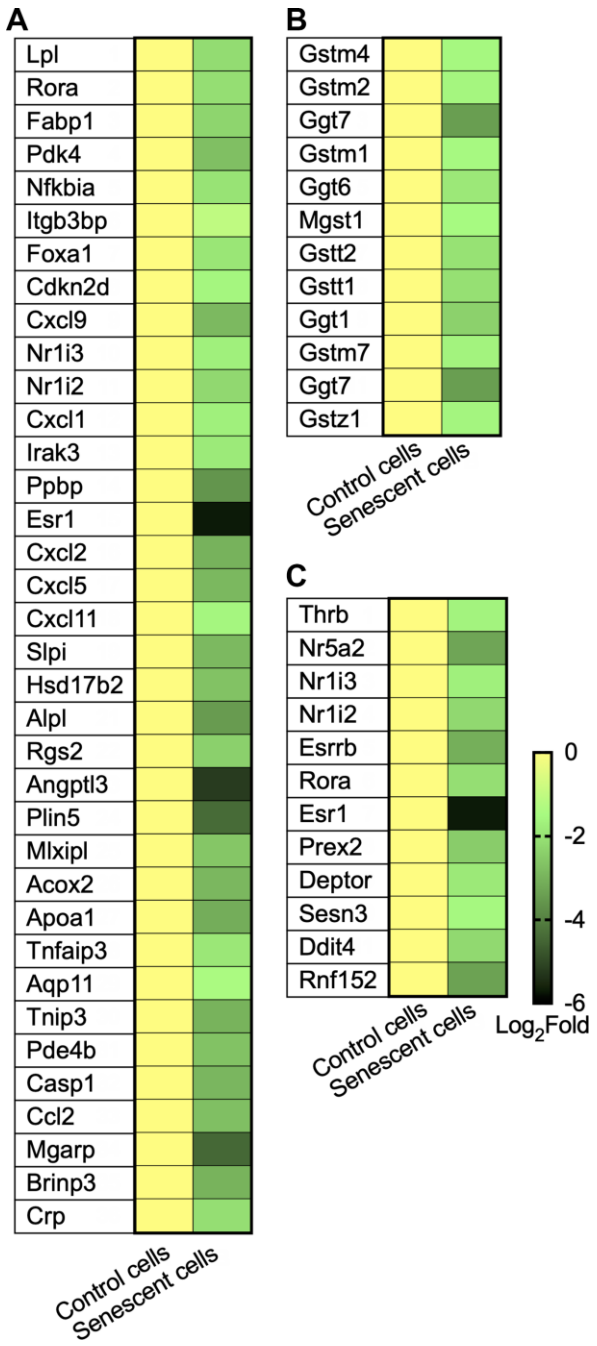

Supplementary Figure 2. RNAseq analysis of control and senescent AML12 cells for downregulated pathways. (**A**) Heat map showing genes regulating pathways: response to lipid (GO:0033993), negative regulation of lipase activity (GO:0060192), lipid homeostasis (GO:0055088), triglyceride homeostasis (GO:0070328), regulation of cholesterol homeostasis (GO:2000188), triglyceride catabolic process (GO:0019433), cellular response to lipid (GO:0071396), negative regulation of lipid storage (GO:0010888), and regulation of lipid biosynthetic process (GO:0046890). (**B**) Heat map showing genes regulating pathways: Glutathione metabolism, Glutathione conjugation Homo sapiens R-HSA-156590, Glutathione synthesis and recycling Homo sapiens R-HSA-174403, glutathione derivative biosynthetic process (GO:1901687), and glutathione metabolic process (GO:0006749). (**C**) Heat map showing genes regulating pathways: Nuclear Receptor transcription pathway Homo sapiens R-HSA-383280, and negative regulation of TOR signaling (GO:0032007).

Supplementary Data

Please browse Full Text version to see the data of Supplementary Data.

Supplementary Data. RNAseq analysis of control and senescent AML12 cells for upregulated and downregulated genes and related pathways.